ENGINEERING RESEARCH JOURNAL (ERJ)

Vol. 1, No. 48 Apr. 2021, pp.337-352

Journal Homepage: http://erj.bu.edu.eg

Numerical investigation of the effect of adding AL_2O_3 nanoparticles to water on bubble formation in a bubble column reactor undergoing vibration.

M. A. I. Wahba[a], Ashraf Mimi Elsaid[b],M. F. Abd- Rabbo[c]

[a]Benha University, Faculty of Engineering at Shoubra, Department of Mathematics and Physics, Cairo, Egypt.

[b]Helwan University, Faculty of Technology and Education, RHVAC Technology Department, Cairo, Egypt.

[c]Benha University, Faculty of Engineering at Shoubra, Department of Mechanical Engineering, Cairo, Egypt.

Key words [Nanoparticles – Vibration -Bubble Column Reactor – Finite Difference Method - Population Balance Equation]

Abstract. Vibration of gas gives an improvement on bubble formation process in bubble column performance. The paper studies the simulation of the bubble size distribution (BSD) in an oscillating bubble column for the air-water system starting from the Population balance equation for water with AL_2O_3 nanoparticles. Two different coalescence models (Prince & Blanch model and Luo model were studied with one breakup model (Martinez-Bazan Breakup) to get the BSD simulation and the Sauter mean diameter at different heights of the column. To get the best coalescence model that would be suitable for the simulation when compared with the experiment and simulation done by Waghmare [18]. Prince and Blanch coalescence model gives very good results when compared with Waghmare [18]. Prince and Blanch model was the best model because it was stable in all frequencies simulations and is recommended for a more complicated vibration model in the future. Then the simulation was done with Prince and Blanch coalescence model, with the same input data, with different percentages of AL_2O_3 nanoparticles in water to investigate the effect of nanoparticles percentage on bubble formation.

1. Introduction

Bubble columns have many engineering applications such as multiphase contractors, petrochemical industry, and chemical industry [1]. Some of the main advantages of Bubble columns that they are compact and have low operating and maintenance costs and can also operate under most conditions of heat and mass transfer rates. Moreover, bubble columns have the ability to add and remove any catalyst and plug-free operation [2]. A bubble column reactor is one type of multiphase reactors, is mainly a cylindrical tube with a gas distributor below the column which pumps gas bubbles into a liquid phase or a liquid–solid suspension. This kind of column has many advantages in designing and working over competitor reactors which results in having a wide application area. During the past two decades, Bubble columns gained high attention because of the massive application field and their industrial importance. Many researchers studied bubble columns with nanoparticles to investigate their effect on the coalescence and breakage process. L. Li et al. [3] made experimental and simulation studies on rising bubbles in a rectangular bubble column with base fluid is methanol and different concentrations of AL_2O_3 nanoparticles. It was found that there will be an increase in both coalescence and breakage with increasing concentration of nanoparticles but with different rates. The increase in coalescence and breakage rate will increase to a certain level in the column, then a decline for both, but the decline rate of coalescence will be larger than breakage rate. F. Su et al. [4] made an experiment to find the effect of nanoparticles on bubble formation, they used a SiO_2-water as a nanofluid, and they found that the bubble will be formed at a higher frequency in nanofluid than in water. Recent research focus on gas holdup studies [5–8], N. Kantarcia et al. [5] said that the properties of the liquid phase strongly affect the gas holdup due to its effect on the formation of bubbles in the bubble column. They found that one of the causes of the formation of larger bubbles is due to increase in liquid viscosity which results in high rise velocities and low gas hold-up. H. Li et al. [9]

designed a heat transfer probe with a high response to determine the coefficient of heat transfer for different velocities of gas and slurry concentrations in a slurry bubble column. They analyzed the turbulent bubble-wake region heat transfer enhancement to know the dynamics of bubble-wake. H. Li et al. [10] made experiments to investigate variations in gas holdups, bubbles velocities, and their populations. They discovered that the increase of slurry concentration up to 25% would decrease the gas holdup and would slightly increase at higher concentrations, and the larger bubbles velocities would increase with slurry concentration up to about 20%, and after that percentage of slurry concentration, it would reach an asymptotic value. R. Schafer et al. [11] discussed the effect of gas, liquid properties, and the operating conditions on the bubble sizes. V.Michele et al. [12] made investigations on flow regime, heat transfer measurements [13]. M. Bouaifi et al. [14] made an experiment to find the volumetric mass transfer coefficient, they found that liquid mass transfer coefficient is dependent on operating conditions. The bubble columns operation types are the semi-batch mode and continuous mode [15]. The main factors affecting the bubble column design are properties of heat and mass transfer, reacting system mixing characteristics, and chemical kinetics. The bubble column performance can be improved by higher Energy input by using vigorous stirring. Many researchers focus on forced oscillations because of their importance in increasing the mass transfer coefficient [16, 17, and 18]. Y. G. Waghmare et al. [18] studies the distribution of bubble size in an oscillating bubble column for a system consisting of air and water with vertical oscillations to raise the performance of the column. He measured bubble size distribution (BSD) at different column heights, considering the effects of important operating parameters like frequency, amplitude, and gas flow rate and he made simulation modeling for Population balance by considering two different breakage kernels (Martinez-Bazan and Luo-Svendsen) and find that Martinez-Bazan is better in his simulation so we take it only in our simulation, he takes only one coalescence kernel (Luo) but it was taken here two kernels in our simulation as will be mentioned later in the rest of the study. K. L. Harbaum et al. [19] studied the effect of sonic vibrations of frequencies 20-2000 c/s on the rate of absorption of carbon dioxide in bubble columns, they found that the main effect of sound is to increase the number of bubbles without a significant change of bubble diameter. R. D. Fawkner et al. [20], studied the effect of changing the frequency (0-60 HZ) on bubble size in pulsed –flow liquids. R. Krishna et al. [21] found out that the bubbles breakage significantly increased when induced by resonance vibrations because of the increase in the interfacial area. There were many attempts made to measure the average bubble size and other properties of bubbles in the oscillating bubble column because of its importance in the engineering field.

The objective of the present work is to study the effect of changing the coalescence kernels in the simulation of forced vibration and solve the population balance equation by the finite difference method on the Sauter mean diameter and the bubble size distribution (BSD). To find the best coalescence kernel that will be suitable in many vibration applications among all the coalescence kernels used here. Then simulate the same input data with the best coalescence kernel on a case of water with different percentages of AL_2O_3 nanoparticles to investigate the effect of adding nanoparticles on the formation of bubbles in A Bubble Column Reactor Undergoing vibration.

2. Population Balance Modeling

In the following work a trail to improve the simulation and the work of Waghmare [18]. The experiment contains a Plexiglas column having a diameter of 8.9 cm and a height of 106 cm. The system operates with frequency from 0-30 Hz and amplitudes from 0 to 2.54 mm. the compressed air was injected into the distilled water in the column from a single capillary injector. A visual photographic technique was used to measure a BSD with a limited gas superficial velocity to a 0.17 cm/s. The bubble volume range was divided into volume classes ($v_{i+1} = 2v_i$), which means the next volume will be twice the previous volume. The number density of bubbles n_i was calculated by the number of bubbles in each volume class (i) per unit volume. The Sauter mean diameter d_{32} which is a measure of mean bubble diameter was calculated from the ratio of the third moment of number density to the second moment as shown in the next equation.

$$d_{32} = \frac{\sum_{i=1}^{N} n_i d_i^3}{\sum_{i=1}^{N} n_i d_i^2} \quad (1)$$

The volume fraction of bubbles of class i/Δd was calculated as follow:

$$\left(\frac{volume\ fraction}{\Delta d}\right)_i = \frac{n_i d_i^3}{(d_i - d_{i-1}) \sum_{i=1}^{N} n_i d_i^3} \quad (2)$$

$$\sum_{i=1}^{N} \left(\frac{volume\ fraction}{\Delta d}\right)_i (\Delta d)_i = 1 \quad (3)$$

But for the present solution and the numerical part in Waghmare [18], both of us use the population Balance Equation for the gas phase which is the theoretical model for the evolution of bubble size distribution. We use here the same numerical technique that Waghmare [18] used in his work, by dividing the gas phase into classes of volume ($v_{i+1} = 2v_i$). The population balance equation is shown in equation (4), the number density of class *i is* n_i is shown in equation (5).

$$\frac{\partial}{\partial t} n_i + \nabla . (u_i n_i) = S_i \quad (4)$$

$$n_i = \frac{\text{number of bubbles in the size class } i}{\text{volume of fluid dispersion}} \quad (5)$$

Where u_i is the rise velocity of the bubble of diameter d_i , rise velocity is dependent on the bubble Diameter, fluid physical properties, vibration frequency, and the kinetic buoyancy Bjerknes force amplitude [18]. As shown by Waghmare [18] the rise velocity can be evaluated from equation (6).

$$K_D \sqrt{\frac{d\rho}{\mu}}\, u^2 + 10\, u^{\frac{3}{2}} - \frac{4}{3} \frac{d^{\frac{3}{2}} \rho^{\frac{1}{2}} g\big(Bj(h)\big)}{\sqrt{\mu}} = 0 \quad (6)$$

$$\big(Bj(h)\big) = \frac{\rho\, h\, A^2\, \omega^4}{2 g p_0} \quad (7)$$

Where K_D is a constant which was taken to fit their data, that parameter was in the drag coefficient equation. $\big(Bj(h)\big)$ is the local Bjerknes number, When the dimensionless local Bjerknes number becomes one, bubble rise velocity becomes zero, that is, the bubble oscillates at a point. Equation (4) is solved numerically, and their numerical results have a good acceptance with their experimental data.

$$S_i = [B_B - D_B + B_C - D_C]_i \quad (8)$$

Where, B_B is the birth of bubble because of bubble breakage, D_B is the death of bubble because of breakage, B_C is the birth of bubble because of coalescence, and D_C is the death of bubble because of coalescence. To get the values of S_i ,which is found in the following equation from Hagesaether [22].

$$B_B(i) = \sum_{k=i+1, i\neq \mathrm{N}}^{N} \Omega_B(k,i) + \sum_{k=1, i\neq \mathrm{N}}^{i} yb_{i+1,k}\Omega_B(i+1,k) + \sum_{k=1, i\neq 1}^{i-1} \big(1 - yb_{i,k}\big)\Omega_B(i,k) \quad , i = 1, \ldots\ldots N \quad (9)$$

$$yb_{i,k} = 2^{1+k-i} \quad for\ k < i \quad (10)$$

$$D_B(i) = \Omega_B(i,k) \quad 2, \ldots\ldots \ldots N \quad (11)$$

$$B_C(i) = \sum_{j=1, i\neq \mathrm{N}}^{i-1} yc_{i,j}\Omega_c(i,j) + \sum_{j=1}^{i-1} (1 - yc_{i-1,j})\Omega_c(i-1,j) \quad , i = 2, \ldots\ldots N \quad (12)$$

$$yc_{i,j} = 1 - 2^{j-i} \quad for\ i \geq j \quad (13)$$

$$D_C(i) = \sum_{j=1}^{N-1} \Omega_c(i,j) + \Omega_c(i,i) \quad i = 1, \ldots\ldots N-1 \quad (14)$$

Where $\Omega_B(i,k)$ is the rate of breakage of bubble d_i to form a bubble d_k and $\Omega_c(i,j)$ is the rate of coalescence of bubbles d_i and d_j . For solving equation (8), there were some assumptions that the bubbles from the smallest class (i=1) will not break and bubbles from the largest class (i =N) will not coalesce. The first term on the right-hand side of equation (8) is the rate of formation of bubble d_i due to the breakage of any bigger bubble d_k when k > i. The next two terms arise due to the redistribution of bubbles. This means that the bubble will break into two daughter bubbles and its volume would distribute among them.

$$v_i = v_l + v_m \quad (15)$$

For example, if we have size classes 1, 2, etc. with corresponding volumes 1, 2, 4, 8, etc. If we assume that $v_i = 8$ would break into $v_l = 7$ and $v_m = 1$,the volume v_m can be directly assigned to size class 1, but v_l would be calculated from equation (16, 17).

$$v_l = yb_{i,k} v_{i-1} + \big(1 - yb_{i,k}\big) v_i \quad (16)$$

$$yb_{i,k} = 2^{1+k-i} \quad for\ k < i \quad (17)$$

In the same way for the coalescence process when a bubble of volume v_i which would be the bigger of the two bubbles coalesces with a bubble of volume v_j , they will form a bubble of v_k by constraint $v_i < v_k < v_{i+1}$. The volume of v_k would be redistributed between v_i and v_{i+1} as follows:

$$v_k = v_i + v_j = yc_{i,j}v_i + (1 - yc_{i,j})v_{i+1} \quad (18)$$

$$yc_{i,j} = 1 - 2^{j-i} \; for \; i \geq j \quad (19)$$

3. Coalescence model

Coalescence is the process by which particles merge during contact to form a new particle. We can get it in terms of particles collision and the probability of their collision will result in coalescence. There were many models published for breakup and coalescence models. The coalescence kernel can be calculated by the product of collision frequency and coalescence efficiency for the physical model [23]. There are many reasons to make collision frequency, such as buoyancy, viscous shear, turbulence, wake entrainment, or capture in turbulent eddies. On the other hand, coalescence efficiency will be due to some other reasons such as the film drainage model, critical velocity model, and energy model. In the present work coalescence kernel made by Prince and Blanch [24], based on the film drainage model will be compared with coalescence model proposed by Luo [25]. A brief explanation of each of the two coalescence kernels will be given in the next words.

3.1 Prince and Blanch

They made their modeling by considering each type of bubble coalescence. They considered bubble collisions created by turbulence, buoyancy, and laminar shear, and by analysis of the coalescence efficiency of collisions [26, 31].

3.1.1 Turbulent collision rate

The turbulent motion collision rate Θ^Tij is dependent on bubble size, concentration, and velocity. The collision of bubbles with each other is due to the collision frequency which results from turbulent motion and the varying velocity of the liquid phase. The turbulent motion collision rate Θ^Tij can be calculated from equation (20):

$$\Theta^T\text{ij} = fi * fj * S_{ij} * (u_{ti} + u_{tj})^{1/2} \quad (20)$$

Where S_{ij} is the cross-sectional area of the bubbles collision which can be calculated from equation (21):

$$S_{ij} = \frac{\pi}{4} * (r_{bi} + r_{bj})^2 \quad (21)$$

The average turbulent velocity in the inertial subrange of isotropic turbulence [28] is:

$$u_t = 1.4 * \epsilon^{\frac{1}{3}} * d^{\frac{1}{3}} \quad (22)$$

By substituting equations (21&22) in equation (20) we get Θ^Tij from equation (23):

$$\Theta^T\text{ij} = 0.089 * \pi * fi * fj * (d_i + d_j)^2 * \epsilon^{\frac{1}{3}} * \left(d_i^{\frac{2}{3}} + d_j^{\frac{2}{3}}\right)^{\frac{1}{2}} \quad (23)$$

3.1.2 Buoyancy-driven collision rates

The bubble buoyancy collision type is caused by the difference in the rise velocity. The buoyant collision rate is calculated from equation (24):

$$\Theta^B\text{ij} = fi * fj * S_{ij} * (u_{ri} - u_{rj}) \quad (24)$$

The bubble rise velocity u_r can be expressed in equation (25) [29]:

$$u_r = \left(\frac{2.14 * \sigma}{\rho d} + 0.505\, gd\right)^{0.5} \quad (25)$$

Where ρ is the fluid density and σ is the surface tension between the gas and the fluid and g is the acceleration of gravity.

3.1.3 Laminar shear collision rate

The laminar shear collision occurs because of the gross circulation development in the column in case of high gas rates. Bubble columns can operate under different hydrodynamic regimes [30]. For low gas flow rates, the gas will be well distributed within the radius of the column. But with higher gas flow rates, there will be an increase in the gross circulation pattern, accompanying a speed to the top in the center of the column and downward speed near the walls. For the high gas flow rates column, the laminar shear collision rate can be calculated from equation (26):

$$\Theta^{LS}\text{ij} = \frac{4}{3} * fi * fj * (r_{bi} + r_{bj})^3 * \left(\frac{dv_l}{dR}\right) \quad (26)$$

Where $\left(\frac{dv_l}{dR}\right)$ is the average shear rate [25, 32], v_l is the velocity of liquid circulation and R is the radial coordinate. The overall coalescence rate from model of Prince & Blanch, is given in equation (27)

$$\Omega\text{c} = (\Theta^T\text{ij} + \Theta^B\text{ij} + \Theta^{LS}\text{ij}) * \exp\left(-\frac{t_{ij}}{\tau_{ij}}\right) \quad (27)$$

$$t_{ij} = \left(\rho \frac{r_{ij}^3}{16\sigma}\right)^{\frac{1}{2}} * \ln\frac{h_0}{h_f} \quad , r_{ij} = \frac{1}{2}\left(\frac{1}{r_{bi}} + \frac{1}{r_{bj}}\right)^{-1} , \quad \tau_{ij} = \frac{r_{ij}^{\frac{2}{3}}}{\epsilon^{\frac{1}{3}}} \quad (28)$$

Where h_0 is the initial film thickness and h_f is the critical film thickness. r_{ij} is the equivalent radius [31]. In the case of mixtures containing surface-active compounds the time of coalescence must be obtained from the film thinning rate [33].

3.2 Luo [25]

Their coalescence rate Ωc was calculated by multiplying the collision frequency $\Theta^{Luo}ij$ with the coalescence Probability $Pc(d_i , d_j)$. Luo considered only the collision frequency due to turbulence, expressed his coalescence probability based on the coalescence theory [18].

$$\Theta^{Luo}ij = 0.089 * \pi * fi * fj * \left(d_i + d_j\right)^2 * \epsilon^{\frac{1}{3}} * \left(d_i^{\frac{2}{3}} + d_j^{\frac{2}{3}}\right)^{\frac{1}{2}} \quad (29)$$

$$Pc(d_i , d_j) = \exp\left(-C \frac{\left[0.75\left(1 + D_j^{*2}\right)\left(1 + D_j^{*3}\right)\right]^{0.5}}{\left(\frac{\rho_G}{\rho} + 0.5\right)^{0.5}\left(1 + D_j^{*}\right)^3} We_{ij}^{0.5}\right) \quad (30)$$

$$D_j^* = \frac{d_j}{d_i}, \quad We_{ij} = \frac{\rho d_i u_{ij}^2}{\sigma}, \quad u_{ij} = \left(u_i^2 + u_j^2\right)^{0.5} , u_i = 1.43(\epsilon\, d_i)^{\frac{1}{3}} \quad (31)$$

$$\Omega c = \Theta^{Luo}ij * Pc(d_i , d_j) \quad (32)$$

Where C is a constant, We_{ij} is Weber number and ρ_G is the gas density. They used the thinning model to calculate coalescence time [34], which would reduce coalescence time by about 10% for a pure air-water system.

4. Break up model

Bubble breaks up when the bubble cannot afford the internal or the external forces created by the fluid, or when the bubble collides with turbulent eddy, which has less or equal size to the bubble size [25, 35, 36, 37]. There are many breakup models, but we choose the breakup model by Martìnez Bazán [38]. Breakage rate $\Omega_B(i,k)$ by Martìnez Bazán can be expressed as in Equation (33).

$$\Omega_B(i,k) = q * b(i) * P_b(i,k) \quad (33)$$

$$b(i) = k_g\, n_i \frac{\left(\beta\,(\epsilon d_i)^{\frac{2}{3}} - \frac{12\,\sigma}{\rho\, d_i}\right)^{0.5}}{d_i} \quad (34)$$

Where q is the number of daughter bubbles produced by the breakup of a parent bubble and in our study we take only binary bubble breakup so q=2, $b(i)$ is the total rate of breakage for a parent bubble of size d_i and $P_b(i,k)$ is the probability that bubble of size d_k will be born due to the breakage of a bubble of size d_i. Where k_g is constant, its value was calculated by Martinez-Bazan [38]. But we take it as 0.55 like Waghmare [18].

The constant β =8.2. We can get an expression for $P_b(i,k)$ from the work of Martinez-Bazan et al [39] which is shown in equation (35).

$$P_b(i,k) = \frac{\left[D_k^{*2/3} - D_{cr}^{*5/3}\right]\left[(1 - D_k^{*3})^{2/9} - D_{cr}^{*5/3}\right]}{\int_{D_{min}^*}^{D_{max}^*}\left[D^{*2/3} - D_{cr}^{*5/3}\right]\left[(1 - D^{*3})^{\frac{2}{9}} - D_{cr}^{*5/3}\right]dD^*} , D_k^* = \frac{d_k}{d_i}, \quad D^* = \frac{d}{d_i} \quad (35)$$

$$D_{cr}^* = \frac{d_{cr}}{d_i} \quad , d_{cr} = \left(\frac{12\sigma}{\beta\rho}\right)^{3/5} \epsilon^{-2/5} \quad , D_{min}^* = \frac{d_{min}}{d_i} \quad , d_{min} = \left(\frac{12\sigma}{\beta\rho\, d_i}\right)^{3/2} \epsilon^{-1} \quad (36)$$

$$D_{max}^* = \frac{d_{max}}{d_i} \quad , d_{max} = d_i\left(1 - \left(\frac{d_{min}}{d_i}\right)^3\right) \quad (37)$$

In our study, we will take the two coalescence kernels with the breakup model by Martìnez Bazán (1999) [38] which is the only breakage kernel we have here which was better in the same operating condition than Luo [25] breakage kernel as mentioned before in Waghmare [18]. The combinations of breakup and coalescence kernels which we use in our simulation are listed in table 1.

5. Solution Methods

The assumption was made that the column operates at the time-averaged periodic steady-state [18]. Also ignoring spatial effects in the radial direction. by these assumptions, equation (4) will become:

$$\left(u_i \frac{d}{dx} n_i\right) = S_i \quad (38)$$

Table 1: Simulation cases

	Kernel combination	Model

Case 1	Martìnez Bazán (1999) Luo	Breakup Coalescence
Case 2	Martìnez Bazán (1999) Prince and Blanch (1990)	Breakup Coalescence

5.1 Finite difference method

Equation (38) will be solved numerically by using finite-difference methods (FDM). By using a backward differencing scheme for equation (38).

$$n_i|_x = n_i|_{x-\Delta x} + \frac{\Delta x}{u_i} S_i \qquad (39)$$

6. Nanofluid equations

When dealing with nanofluid simulation, there will be changes in the values of the properties of the fluid, so the properties of the nanofluid will be calculated from the following equations.

Density equation of the (AL_2O_3-water) Nano fluid is given by [40]:

$$\rho_{nf} = (1 - \Phi)\, \rho_{bf} + \Phi\, \rho_p \qquad (40)$$

Where ρ_{nf} is nanofluid density, ρ_{bf} is the water density, ρ_p is the nanoparticles density and Φ the nanoparticles volume fraction.

The dynamic viscosity equation was proposed by Brinkman model for a (AL_2O_3-water) Nanofluid is given by [40]:

$$\mu_{nf} = \frac{\mu_f}{(1 - \Phi)^{2.5}} \qquad (41)$$

Where μ_{nf} is the nanofluid viscosity, μ_f is the water viscosity.

Table 2 Thermophysical properties of different phases [40, 41].

Physical properties	**Fluid phase (water)**	**Nanoparticles (Al_2O_3)**
ρ (kg/m^3)	997	3970
μ (kg m^{-1}s^{-1})	0.001004	-
σ (N/m)	0.0726	-

For the surface tension (σ), its results were taken from an experimental data curve [41] and the values were (for 1% AL_2O_3, σ=0.073 & for 2% AL_2O_3, σ=0.07355)

7. Results Verifications

Population balance equation simulations were done for an oscillatory bubble column at three different frequencies (15, 17.5, and 20 Hz) with constant amplitude (1.66 mm) and constant superficial gas velocity (0.17 cm/s) like the simulation in [18]. The boundary condition needed to solve the population equation (45) and (56) was taken almost the same trend that was taken as the Experimental BSD at a height (H) of 10.6 cm above the injector [18].

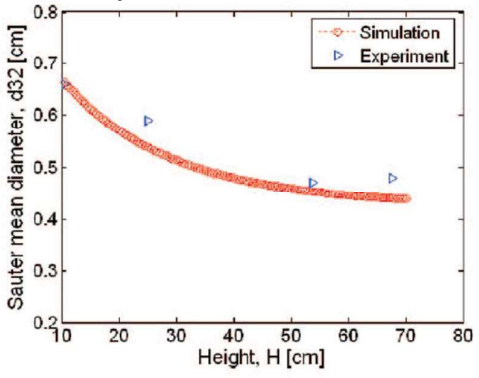

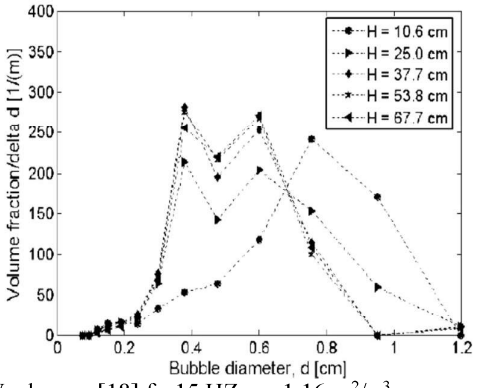

(a1) Waghmare [18],f =15 HZ ,ϵ =1.16 m^2 / s^3(a2)Waghmare [18],f =15 HZ ,ϵ =1.16 m^2/ s^3

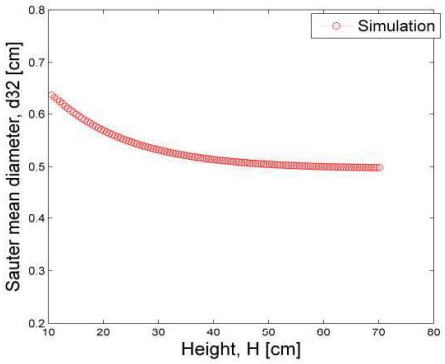

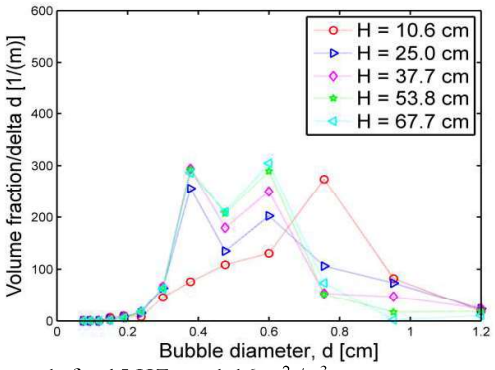

(a11) case 1, f =15 HZ, ϵ =1.16 m^2 / s^3 (a22) case 1, f = 15 HZ, ϵ =1.16 m^2 / s^3

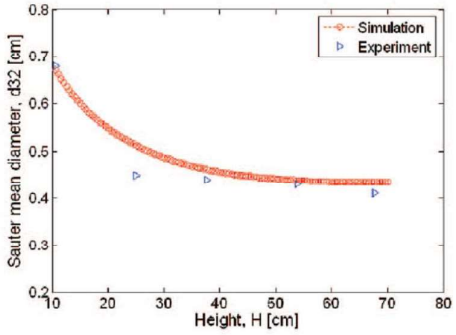

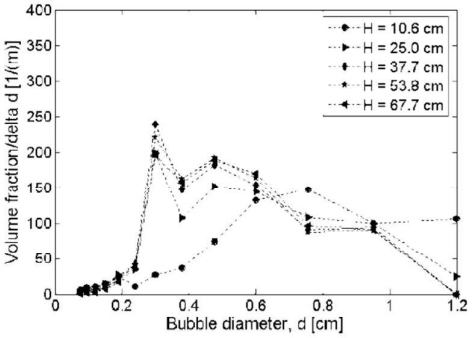

(b1) Waghmare [18], f = 17.5 HZ, ϵ =1.85 m^2 / s^3 (b2) Waghmare [18],f = 17.5 HZ ,ϵ =1.85 m^2 / s^3

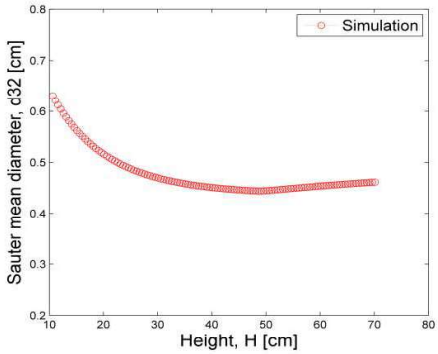

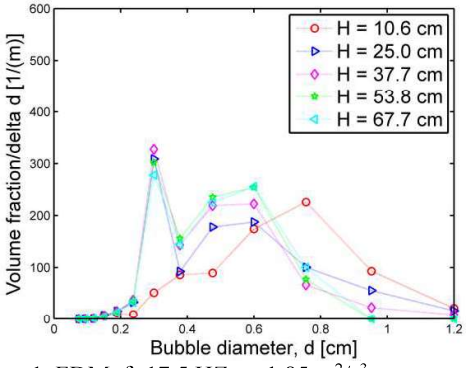

(b11) case 1, FDM, f=17.5 HZ, ϵ =1.85 m^2/s^3 (b22) case 1, FDM, f=17.5 HZ, ϵ=1.85 m^2/s^3

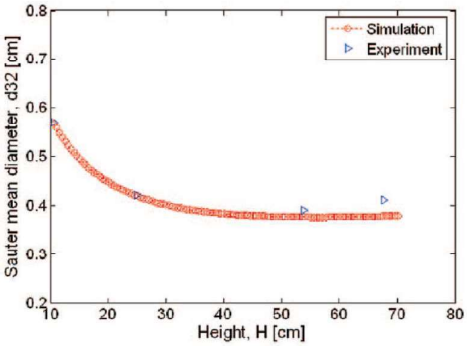

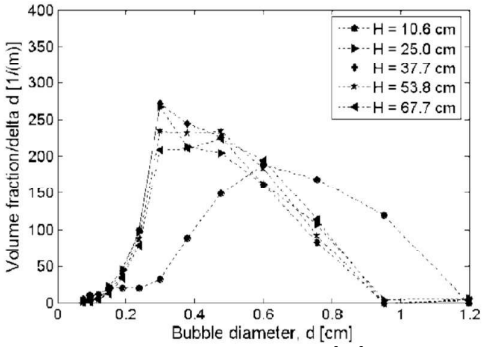

(c1) Waghmare [18], f =20 HZ, ϵ=2.75 m^2 / s^3(c2) Waghmare [18], f =20 HZ ,ϵ=2.75 m^2/s^3

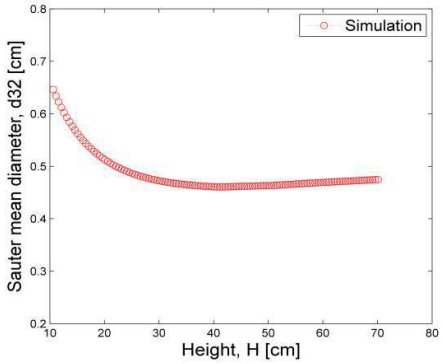

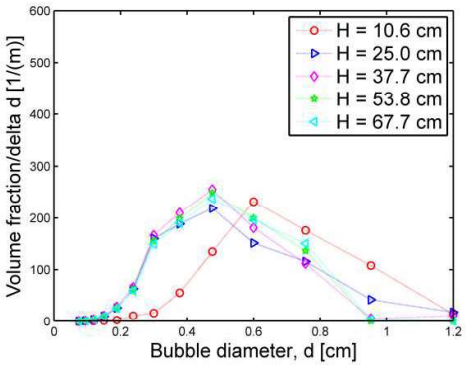

(c11) case 1, f = 20 HZ, ϵ =2.75 m^2 / s^3 (c22) case 1, f = 20 HZ, ϵ =2.75 m^2 / s^3

Figure.1. Comparison between predicted and observed values of Sauter mean diameter as a function of height in the figures (a1,b1,c1) & Evolution of bubble size distribution at different heights in the column in the figures (a2,b2,c2) .

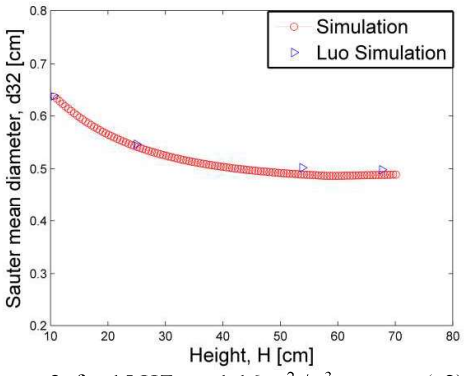

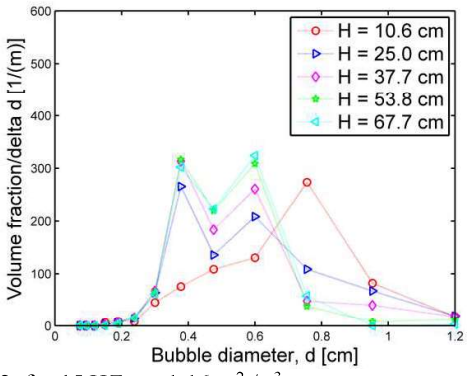

(a1) case 2, f = 15 HZ, ϵ =1.16 m^2 / s^3 (a2) case 2, f = 15 HZ, ϵ =1.16 m^2 / s^3

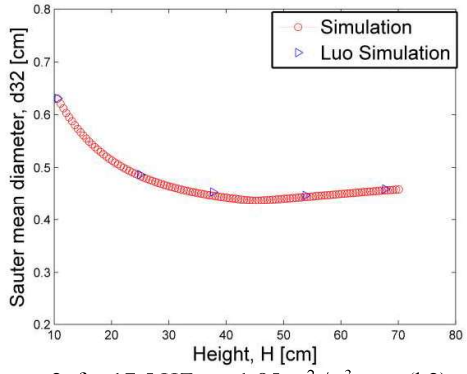

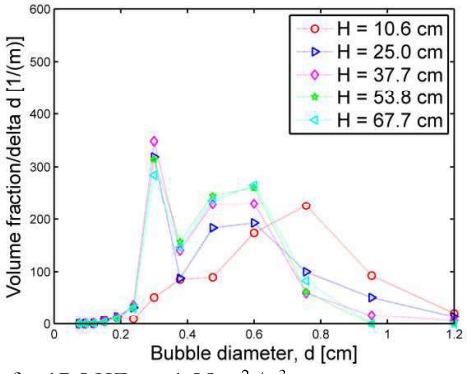

(b1) case 2, f = 17.5 HZ, ϵ =1.85 m^2 / s^3 (b2) case 2, f = 17.5 HZ, ϵ =1.85 m^2 / s^3

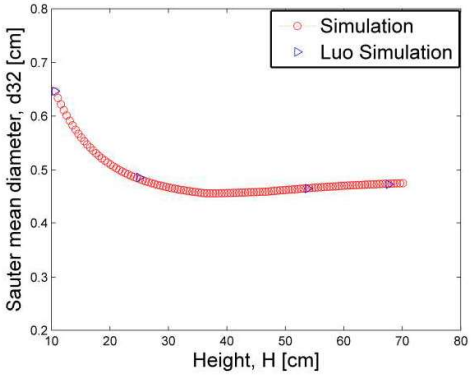

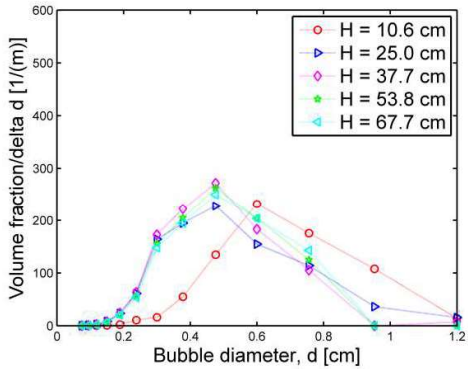

(c1) case 2, f = 20 HZ, ϵ =2.75 m^2 / s^3 (c2) case 2, f = 20 HZ, ϵ =2.75 m^2 / s^3

Figure.2 Comparison between case 2 simulation and Leo simulation of Sauter mean diameter as a function of height in the figures (a1,b1,c1) & Evolution of bubble size distribution at different heights in the column in the figures (a2,b2,c2) .

The simulation results are divided into two parts, first part is to compare the two coalescence kernels, to find which one of them is better in vibration simulations. The second part is to simulate with the best coalescence kernel and the same inputs, but with (AL_2O_3-Water) nanofluid, to see the effect of adding nanofluid particles to the water on the simulations.

All the results in the first part are shown in the drawing from figure (1&2), the population balance equation was solved by the finite difference method (FDM) with Δh= 0.005 m(the length of the step in simulating finite difference method, this value will be used in all our simulation in this paper) for the two cases which were shown in table (1), all the cases were studied at different frequencies (15 HZ, 17.5 HZ, 20 HZ) at the same amplitude (A= 1.66 mm) and the same superficial gas velocity (Uog = 0.17 cm/s). The energy dissipation rate (ϵ) was different according to the frequency. Our work was divided into two sections one to make our comparing results with Waghmare [18]. First, our simulation was done using Leo coalescence kernel and compare our results with the corresponding results in Waghmare [18]. Because we have not their results in numbers, we assume a close number to their results. So, my results will take their trend in all frequencies simulation. If that was done, I will proceed to the next step and compare all coalescence kernels. From figure (1) (a1&a11) at 15 HZ it is seen that our results have the same trend as the results from Waghmare work [18]., the same thing happened in figure (1) (b1&b11) for 17.5 HZ and finally in figure (1) (c1&c11) for 20 HZ. So, for all different frequencies, our simulation gives the same trend.

8. Results and Discussion

After the verification of the present results with Waghmare [18] results in figure (1). So, moving to the next step in our paper is to simulate the same problem with the other two coalescence kernels at different frequencies to see if the kernels are suitable for Bubble Column Reactor Undergoing vibration and if not suitable, we multiply it with a factor to make it suitable like what Waghmare [18] done with Leo coalescence kernel to make it suitable for Bubble Column Reactor Undergoing vibration.

Then discuss the results of case 2 as we can see in figure (2) the results were in a very good match to case 1, where the blue point is case (1) simulation in figure (1) (a1, b1, c1) for frequencies 15 HZ, 17.5 HZ, and 20 HZ, respectively.

The prince Coalescence Model was not modified, and the results were very well matched to the case 1 results because this model was proposed for the rates of bubble coalescence and bubble breakup in turbulent gas-liquid dispersions. Prince Bubble coalescence is modeled by considering bubble collisions due to turbulence, buoyancy, and laminar shear, and by analysis of the coalescence efficiency of collisions. So, he made his model in circumstances close to the vibration here in columns. That is why his results were very close to case (1) results.

It was found from a simulation that the prince Coalescence Model does not need any modification to simulate vibration in bubble column because it is suitable for turbulent flow. And the best in the two models in simulation results was Prince and Blanch (1990) because it was stable in all frequencies simulations.

8.1 Nanofluid simulation

In this part of the paper, we will compare the simulation results of water with the simulation results of the (AL_2O_3-water) Nanofluid for the Sauter mean diameter vs height and the volume fraction vs. bubble diameter to see if adding the (AL_2O_3) Nanoparticles will change the Sauter mean diameter or the volume fraction of the bubble.

First starting with 15 HZ. In figure (3) (a1) when simulating water versus 1% AL_2O_3 nanoparticles in (AL_2O_3-water) Nanofluid, there is a very small difference in the Sauter mean diameter between the two cases. If we magnify the figure, we will see that there a very small amount of increase in the Sauter mean diameter (that means an increase in the coalescence of bubble over breakage) from the beginning in an increasing effect then a decay effect until it reaches 33.6883 cm column height, where at this height the Sauter mean diameter of water will equal to that of 1% AL_2O_3 nanoparticles in (AL_2O_3-water) Nanofluid. Then there is a very small decrease in the values of the Sauter mean diameter of 1% AL_2O_3 nanoparticles in (AL_2O_3-water) Nanofluid to that of water (that means an increase in breakage over coalescence from 33.69 cm to the end of the column). To see how the results are very close between water and 1% AL_2O_3 nanoparticles, look at the water d32 [cm] mean value 0.5293 with d32 standard deviation of 0.03666[cm], and for 1% AL_2O_3

nanoparticles d32 [cm] mean value 0.5292 with d32 standard deviation of 0.03686[cm]. That means there is a very small effect of Nanofluid with that percentage. But in overall there is an increase in the breakage process because of the decrease in the d32 mean value of 2% AL_2O_3 nanoparticles than the water mean value.

This case like what was happened in [3], when there was an increase in both coalescence and breakage to a certain level of the column, and then decay in both coalescence and breakage increase in the rest of the column, but the results are in the favor of breakage over coalescence after that point.

then in figure (3) (b1) when simulating water versus 2% AL_2O_3 nanoparticles in (AL_2O_3-water) Nanofluid, there is a much different than 1% AL_2O_3 nanoparticles, but still, a small difference in the Sauter mean diameter between the two cases. we can see from the figure that there is a seen small amount of increase in the Sauter mean diameter (that means an increase in the coalescence of bubble over breakage) from the beginning in an increasing effect then a decay effect until it reaches 51.2188 cm column height, where at this height the Sauter mean diameter of water will equal to that of 2% AL_2O_3 nanoparticles in (AL_2O_3-water) Nanofluid. Then there is a small decrease in the values of the Sauter mean diameter of 2% AL_2O_3 nanoparticles in (AL_2O_3-water) Nanofluid to that of water (that means an increase in breakage over coalescence from 51.2185 cm to the end of the column). To see how the results are very close between water and 2% AL_2O_3 nanoparticles, look at the water d32 [cm] mean value 0.5293 with d32 standard deviation of 0.03666[cm], and for 2% AL_2O_3 nanoparticles d32 [cm] mean value 0.5296 with d32 standard deviation of 0.03687[cm]. That means there is a very small effect of Nanofluid with that percentage. But overall, there is an increase in the coalescence process because of the increase in the d32 mean value of 2% AL_2O_3 nanoparticles over the water mean value. This also likes what was happened in [3] but with a higher height level. We could conclude that at 15 HZ the increase in nanoparticle percentage will increase the column height at which the Sauter mean diameter of water will equal to that of (AL_2O_3-water) Nanofluid. Then after that, there will be a decrease in the Sauter mean diameter of (AL_2O_3-water) Nanofluid to that of water to the end of the column. Figure (3) (c) shows all Sauter mean diameter simulations for water,1%AL_2O_3 nanoparticles, and 2%AL_2O_3 nanoparticles, it is seen from that figure that for the two values of Nanofluid there is a small change in coalescence and breakage.

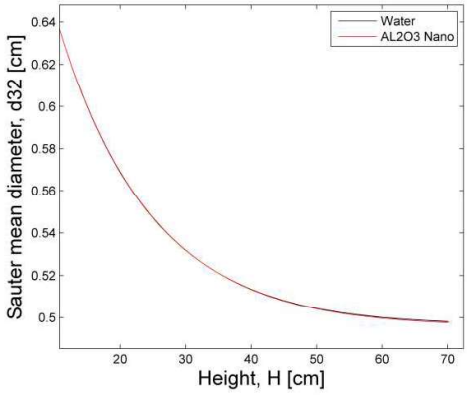

(a1) Sauter mean diameter for water and 1% AL_2O_3 Nanofluid at f = 15 HZ

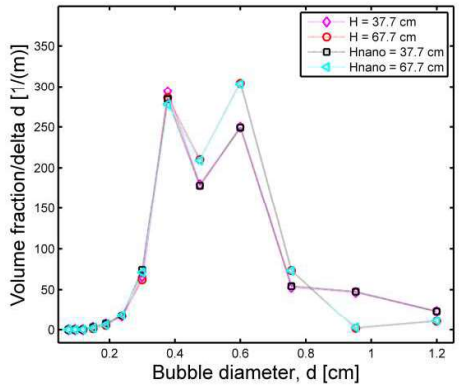

(a2) bubble size distribution at different heights for water and 1% AL_2O_3 Nanofluid at f = 15 HZ

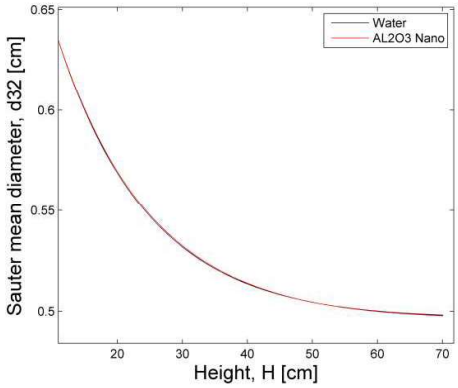

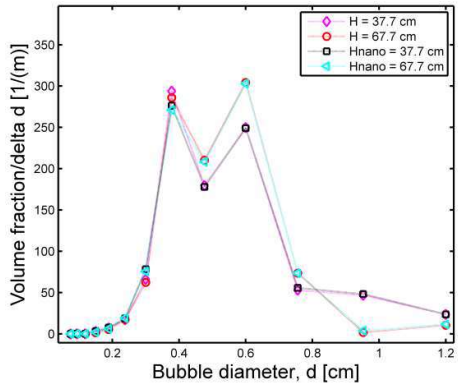

(b1) Sauter mean diameter for water and 2% AL_2O_3 Nanofluid at f = 15 HZ (b2) bubble size distribution at different heights for water and 2% AL_2O_3 Nanofluid at f = 15 HZ

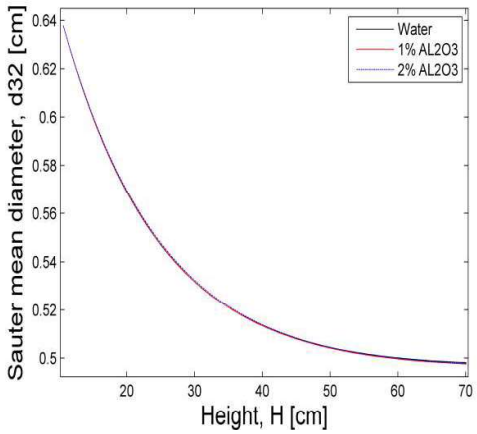

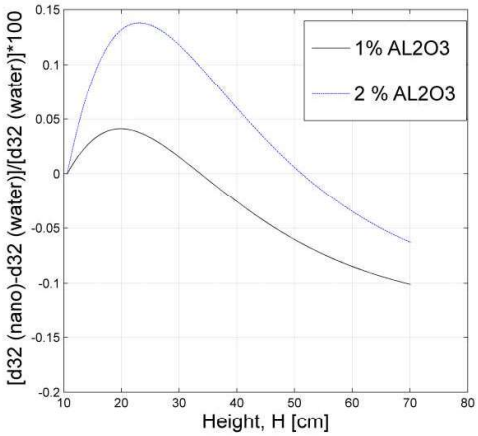

(c) Sauter mean diameter for water and different percentage AL_2O_3 Nanofluid at f = 15 HZ (d) Sauter mean diameter increase and decrease percentage for different percentage AL_2O_3 Nanofluid at different column height for f = 15 HZ.

Figure. 3 Comparison between the values of Sauter mean in water and AL_2O_3 Nanofluid at a different percentage of Nanoparticles (a1,b1) & Evolution of bubble size distribution at different heights in the column for water and AL_2O_3 Nanofluid at a different percentage of Nanoparticles in the figures (a2,b2).

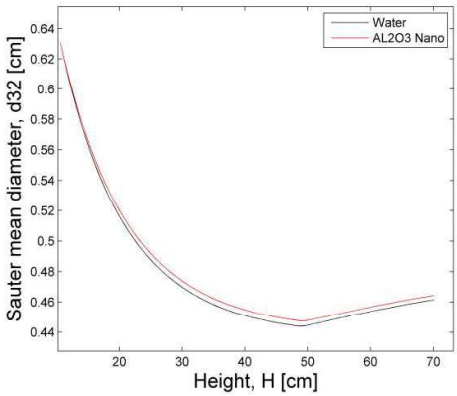

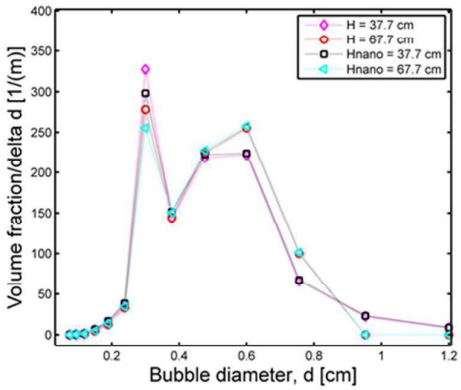

(a1) Sauter mean diameter for water and 1% AL_2O_3 Nanofluid at f = 17.5 HZ (a2) bubble size distribution at different heights for water and 1% AL_2O_3 Nanofluid at f = 17.5 HZ

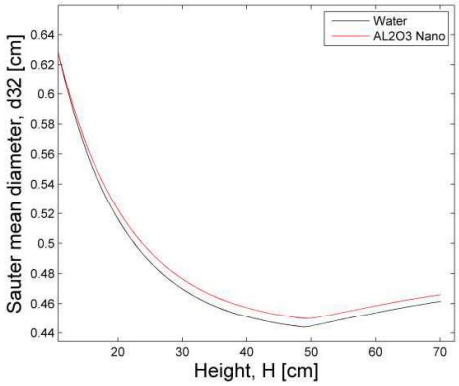

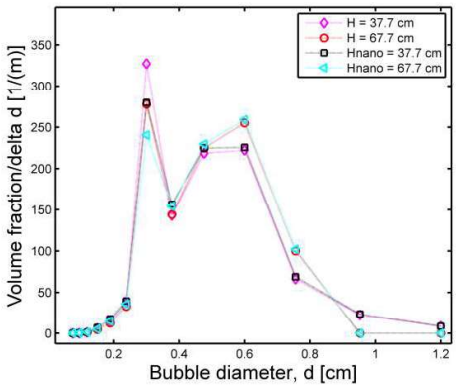

(b1) Sauter mean diameter for water and 2% AL_2O_3 Nanofluid at f = 17.5 HZ (b2) bubble size distribution at different heights for water and 2% AL_2O_3 Nanofluid at f = 17.5 HZ.

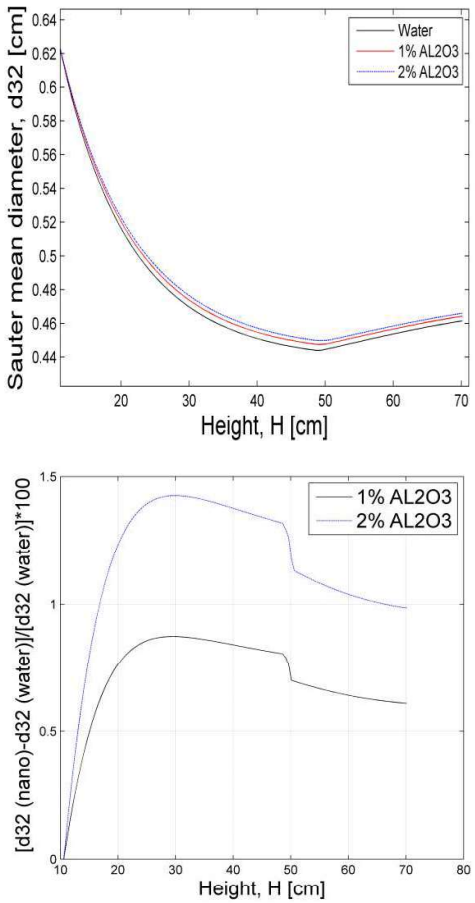

(c) Sauter mean diameter for water and different percentage of AL_2O_3 Nanofluid at f = 17.5 HZ.
(d) Sauter mean diameter increase and decrease percentage for different percentage AL_2O_3 Nanofluid at different column height for f = 17.5 HZ.

Figure. 4 Comparison between the values of Sauter mean in water and AL_2O_3 Nanofluid at a different percentage of Nanoparticles (a1, b1) at f = 17.5 HZ & Evolution of bubble size distribution at different heights in the column for water and AL_2O_3 Nanofluid at a different percentage of Nanoparticles in the figures (a2, b2) at f = 17.5 HZ.

Figure (3) (d) shows the percentage increase and decrease in Sauter mean diameter with changing percentage of AL_2O_3 nanoparticles, it is seen from that figure that for 1%AL_2O_3 a maximum difference between the Sauter mean diameter of nanofluid and the Sauter mean diameter of water at height of 20.1 cm with an increase of 0.041 percentage and with maximum breakage at 70 cm with an increase of 0.101 percentage. From the same figure for 2%AL_2O_3, a maximum difference between the Sauter mean diameter of nanofluid and the Sauter mean diameter of water at height of 23.1 cm with an increase of 0.1379 percentages and with maximum breakage at 70 cm with an increase of 0.063 percentages. So, there is no benefit from using Nanofluid at this percentage to increase coalescence or breakage.

Then looking at the 17.5 HZ simulation. In figure (4) (a1) when simulating water versus 1% AL_2O_3 nanoparticles in (AL_2O_3-water) Nanofluid, there is a seen difference in the Sauter mean diameter between the two cases. it is obvious that there is a shifting of the 1%AL_2O_3 curve up, which means there is a seen increase in coalescence process over breakage process in all length of the column. But with small amount increase in coalescence, to see how the results are close between water and 1% AL_2O_3 nanoparticles, look at the water d32[cm] mean value 0.4774with d32 standard deviation of 0.044 [cm], and for 1% AL_2O_3 nanoparticles d32[cm] mean value 0.4807with d32 standard deviation of 0.0436 [cm].

Then in figure (4) (b1) when simulating water versus 2% AL_2O_3 nanoparticles in (AL_2O_3-water) Nanofluid, there is a more seen difference in the Sauter mean diameter between the two cases. From the figure, there is also a shifting of the 2%AL_2O_3 curve up more than the 1%AL_2O_3, which means there is a more seen increase in coalescence process over breakage process in all length of the column. But with small amount increase in coalescence, to see how the results are close between water and 2% AL_2O_3 nanoparticles, look at the water d32[cm] mean value 0.4774with d32 standard deviation of 0.044 [cm], and for 2% AL_2O_3 nanoparticles d32[cm] mean value 0.4828 with d32 standard deviation of 0.0434 [cm]. When comparing the results of 17.5 HZ with 15 HZ, we find that the 17.5 results are more seen and have only coalescence processes which are increased with increasing nanoparticle percentage.

Figure (4)(c) shows all Sauter mean diameter simulations for water,1%AL_2O_3 nanoparticles, and 2%AL_2O_3 nanoparticles, it is seen from that figure that for the two values of Nanofluid there is a seen increasing change in coalescence process over the breakage process with increasing the percentage of nanoparticles. Figure (4)(d) shows the percentage increase and decrease in Sauter mean diameter with changing percentage of AL_2O_3 nanoparticles, it is seen from that figure that for 1%AL_2O_3 a maximum difference between the Sauter mean diameter of nanofluid and the Sauter mean diameter of water at height of 29.6 cm with an increase of 0.8735 percentage. From the same figure for 2%AL_2O_3, a maximum difference between the Sauter mean diameter of nanofluid and the Sauter mean diameter of water at height of 20.1 cm with an increase of 1.4263 percentages.

We conclude for 17.5 HZ that the increase in the percentage of AL_2O_3 nanoparticles will increase

the Sauter mean diameter overall the column, that means to increase the coalescence process over the breakage process in all the column with a maximum increase of 1.4263 percentage for 2% AL_2O_3 and a maximum increase of 0.8735 percentage for a 1% AL_2O_3. So, there is benefit from using Nanofluid at this percentage to increase the coalescence process over the breakage process.

9. Conclusions

The effects of low frequency and low amplitude fluid vibrations on the BSD in a bubble column reactor filled with water and AL_2O_3 nanoparticles were studied. In the present work, the work done by Waghmare [18] was improved by doing the simulation with two different coalescence models (Prince and Blanch (1990) and Luo (which was used in his simulation)) with the breakup model (Martinez-Bazan Breakup (MB)) which was recommended in his work. It was found from the simulation that the prince Coalescence Model does not need any modification to simulate vibration in bubble column because it is suitable for turbulent flow. Prince and Blanch (1990) was the best because it was stable in all frequencies simulations and are recommended for a more complicated vibration model in the future.

For the simulation of bubbles in nanofluid undergoing vibration. For a 15 HZ the increase in nanoparticle percentage will increase the column height at which the Sauter mean diameter of water will equal to that of (AL_2O_3-water) Nanofluid. Then after that, there will be a decrease in the Sauter mean diameter of (AL_2O_3-water) Nanofluid to that of water to the end of the column. There is a small change in coalescence and breakage. So, there is no benefit from using Nanofluid at this percentage to increase coalescence or breakage. For a 17.5 HZ the increase in the percentage of AL_2O_3 nanoparticles will increase the Sauter mean diameter overall the column, that means increase the coalescence process over the breakage process in all the column. So, there is benefit from using Nanofluid at this percentage to increase the coalescence process over the breakage process.

Nomenclature

n_i number of bubbles in each volume class (i) per unit volume of dispersion

u_i is the rise velocity of bubble of diameter d_i ,m/s

d_{32} is The Sauter mean diameter,m

v_i is the volume class i , m^3

$yc_{i,j}$ is the redistribution factor for coalescence, dimensionless

S_i is the source term that is dependent on coalescence and breakage of bubble class i

fi is the number of bubbles in class i, dimensionless

K_D is an adjustable parameter, dimensionless.

fj is the number of bubbles in class j, dimensionless

$Bj(h)$ is the local Bjerknes number, dimensionless

$Pc(d_i, d_j)$ is the coalescence efficiency, dimensionless

f is the frequency, Hz

A is the amplitude imposed by liquid pulsation, m

ρ is the fluid density, kg/m3

h is the liquid column height above the datum point, m

σ is the surface tension between the gas and the fluid, N/m

ω is the frequency, radians/s

r_{bi} is the bubble radius of class i , m

α is the gas hold-up, dimensionless

r_{bj} is the bubble radius of class j , m

p_0 is the atmospheric pressure, N/m2

S_{ij} is the cross-sectional area of the bubbles collision, m2

g is the acceleration due to gravity, m/s2

u_t is the average turbulent velocity, m/s

μ is the liquid viscosity, Pa · s

u_r is the bubble rise velocity, m/s

B_B is the birth of bubble due to bubble breakage, 1/(m3 · s)

ϵ is the energy dissipation per unit mass, m2/s3

D_B is the death due to breakage, 1/(m3 · s

h_0 is the initial film thickness, m

B_C is the birth due to coalescence, 1/(m3 · s)

h_f is the critical film thickness, m

D_C is the death due to coalescence, 1/(m3 · s)

r_{ij} is the equivalent radius, m

$\Omega_B(i,k)$ is the rate of breakage of bubble d_i to form a bubble d_k, 1/(m3 · s)

t_{ij} is bubble coalescence time, s

$\Omega_c(i,j)$ is the rate of coalescence of bubbles d_i and d_j , 1/(m3 · s)

τ_{ij} is the bubbles contact time, s

ω is the frequency, radians/s

ρ_G is the gas density, kg/m3

θij is the collision rate, 1/(m3 · s)

q is the number of daughter bubbles produced by the breakup of a parent bubble, dimensionless

$yb_{i,k}$ is the redistribution factor for breakage, dimensionless

b(i) is the total rate of breakage for a parent bubble of size d_i, 1/(m3 · s)

$P_b(i,k)$ is the probability that a bubble of size d_k will be born due to the breakage of a bubble of size d_i, dimensionless

Re is the Reynolds number, dimensionless

β is a constant, dimensionless

k_g is a constant, dimensionless

$D^*$is the dimensionless bubble diameter

t is the time, s

x is a spatial variable, m

Uog is the superficial gas velocity, m/s

Δh is the change in height, m

References

[1] S. Degaleesan, M. Dudukovic and Y. Pan, "Experimental study of gas induced liquid-flow structures in bubble columns," AIChE Journal 47, 2001, pp.1913–1931.

[2] A.Prakash, A.Margaritis, H.Li and M.A Bergougnou, "Hydrodynamics and local heat transfer measurements in a bubble column with suspension of yeast," Biochemical Engineering Journal 9, 2001, pp. 155–163.

[3] L. Li and Y. T. Kang, "Effects of bubble coalescence and breakup on CO2 absorption performance in nanoabsorbents," Journal of CO2 Utilization 39, 2020, 101170.

[4] F. Su, X. Ma and J. Chen, Effect of nanoparticles on forming process of bubbles in a nanofluid, ASME 2009 2nd Micro/Nanoscale Heat & Mass Transfer International Conference December 18-22, 2009, Shanghai, China.

[5] N. Kantarcia , F. Borakb and K. O. Ulgena, "Bubble column reactors," Process biochemistry 40(7), 2005, pp.2263-2283.

[6] M.Z.A.Anabtawi ,S.I.Abu-Eishah ,N.Hilal and M.B.W.Nabhan , "Hydrodynamic studies in both bi-dimensional and three-dimensional bubble columns with a single sparger," Chem Eng Process ,2002, pp.1–6.

[7]S.Wanga,Y.Arimatsu,K.Koumatsu,K.Furumoto,M.Yoshimoto,K.Fukunaga and K.Nakaoa ,"Gas holdup, liquid circulating velocity and mass transfer properties in a mini-scale external loop airlift bubble column," Chem Eng Sci 58, 2003, pp.3353–3360.

[8] A.Forret ,J-M .Schweitzer , T.Gauthier ,R.Krishna and D.Schweich," Influence of scale on the hydrodynamics of bubble column reactors: an experimental study in columns of 0.1, 0.4 and 1 m diameters," Chem Eng Sci 58, 2003, pp.719–724.

[9] H. Li and A. Prakash,"Analysis of bubble dynamics and local hydrodynamics based on instantaneous heat transfer measurements in a slurry bubble column," Chem Eng Sci54, 1999, pp.5265–5271.

[10] H. Li and A. Prakash," Influence of slurry concentrations on bubble population and their rise velocities in three-phase slurry bubble column," Powder Technol 113, 2000, pp.158–167.

[11] R. Schafer, C. Marten and G. Eigenberger,"Bubble size distributions in a bubble column reactor under industrial conditions," Exp Therm Fluid Sci 26, 2002, pp.595–604.

[12] V.Michele and D.C. Hempel," Liquid flow and gas holdup-measurement and CFD modeling for two-and-three-phase bubble columns, " Chem Eng Sci 57, 2002, pp.1899–1908.

[13] W. Chen, T. Hasegawa, A. Tsutsumi, K. Otawara and Y. Shigaki, "Generalized dynamic modeling of local heat transfer in bubble columns, " Chem Eng J 96, 2003, pp.37–44.

[14] M. Bouaifi, G. Hebrard, D. Bastoul and M. Roustan, "A comparative study of gas holdup, bubble size, interfacial area and mass transfer coefficients in stirred gas–liquid reactors and bubble columns, " Chem Eng Process 40, 2001, pp.97–111.

[15] L. Z. Pino, R.B. Solari, S. Siuier, L. A. Estevez, M.M. Yepez and A.E .Saez, " Effect of operating conditions on gas holdup in slurry bubble columns with a foaming liquid, " Chem Eng Commun117, 1992,pp,367–382.

[16] F. C. Knopf, J. Ma, R. G. Rice and D. Nikitopoulos, "pulsing to improve bubble column performance: I. Low gas rates. " AIChE J 52 (3), 2006, PP. 1103–1115.

[17] F. C. Knopf, Y. Waghmare J. Ma, and R. G. Rice, "Pulsing to improve bubble column performance: II. Jetting gas rates, " AIChE J. 52 (3), 2006, pp.1116–1126.

[18] Y. G. Waghmare, C. A. Dorao, H. A. Jakobsen, F. Carl Knopf, and R. G. Rice, "Bubble Size Distribution for A Bubble Column Reactor Undergoing Forced Oscillations," American Chemical Society, 2009, pp. 1786–1796.

[19] K. L.Harbaum, and G. Houghton, "Effects of sonic vibrations on the rate of absorption of carbon dioxide in gas bubble-beds, " J. appl. Chem.12 (5), 1962, pp. 234-240.

[20] R. D. Fawkner, P. Kluth, and J. Dennis, "Bubble Formation at Orifices in Pulsed, Flowing Liquids, "Chem. Eng. Res. Des. 68 (1), 1990, pp. 69–73.

[21] R. Krishna, J. Ellenberger, M. I.Urseanu, and F. J Keil, "Utilisation of bubble resonance phenomena to improve gas-liquid contact, " Naturwissenschaften 87 (10), 2000, pp. 455–459.

[22] L.Hagesaether, H. A.Jakobsen, and H. F. Svendsen, "Modeling of the dispersed-phase size distribution in bubble columns, " Ind. Eng. Chem. Res. 41 (10), 2002,pp. 2560–70.

[23] F. Lehr, M. Millies, and D. Mewes, "Bubble-Size distributions and flow fields in bubble columns , " Aiche Journal 48(11), 2002,pp. 2426-2443.

[24] M. J. Prince and H. W. Blanch, "Bubble Coalescence and Break-up in Air-Sparged Bubble- Columns, " Aiche Journal 36(10), 1990, pp. 1485-1499.
[25] H. Luo, Coalescence, breakup and liquid circulation in bubble column reactors. D.Sc. Thesis, Norwegian Institute of Technology, Trondheim, Norway, 1993.
[26] P.G.Saffman, and J.S. Turner, "On the collision of drops in turbulent clouds. " Journal of Fluid Mechanics, 1956, pp.16-30.
[27] A.K. Chesters, "The modelling of coalescence processes in fluid-liquid dispersions, " Trans IChemE 69, 1991.
[28] M. Bouaifi, G. Hebrard, D. Bastoul, and M. Roustan, "A comparative study of gas holdup, bubble size, interfacial area and mass transfer coeffi- cients in stirred gas–liquid reactors and bubble columns, " Chem Eng Process40, 2001, pp.97–111.
[29] R.Clift, J. R. Grace, and M. E. Weber, Bubbles, Drops and Particles, Academic Press, New York (1978).
[30] Y. T.Shah, and W. D. Deckwer, Hydrodynamics of Bubble Columns, Handbook of Fluids in Motion, Ann Arbor Science Publishers, Ann Arbor, MI, 583 ,1983.
[31] A. K.Chesters, and G. Hofman, "Bubble Coalescence in Pure Liquids, " Appl. Scientif. Res.38, 1982, pp. 353–361.
[32] A. Laari, and I. Turunen, "Experimental Determination of Bubble Coalescence and Break-up Rates in a Bubble Column Reactor, " The Canadian Journal of Chemical Engineering 81, 2003.pp. 395-401.
[33] T. Oolman, and H.W. Blanch, "Bubble Coalescence in Air-Sparged Bioreactors, " Biotech. Bioeng. 28, 1986, pp.578–584.
[34] R. G. Rice, "Analytical Solutions for Film Thinning Dynamics in Bubble Coalescence." AIChE J. 52 (4), 2006, PP. 1621–1622.
[35] L. Deju, S. C. P. Cheung, G. H. Yeoh and J. Tu, An assessment of mechanistic breakage and coalescence kernels in poly-dispersed multiphase flow,Ninth International Conference on CFD in the Minerals and Process Industries CSIRO, Melbourne, Australia, 2012.
[36] F. Lehr, M. Millies, and D. Mewes, "Bubble-Size Distributions and Flow Fields in Bubble Columns," AIChE Journal 48, 2002, pp. 2426-2443.
[37] H. Luo and H. F. Svendsen, "Theoretical Model for Drop and Bubble Breakup in Turbulent Dispersions," AIChE JOURNAL 42, 1996, pp. 1225-1233.
[38] C. Martínez-Bazán,J. L. Montañés and J. C. Lasheras , "On the breakup of an air bubble injected into a fully developed turbulent flow. Part 1. Breakup frequency, " J. Fluid Mech. 401, 1999, pp. 157–182.
[39] C. Martínez-Bazán,J. L. Montañés and J. C. Lasheras, "On the breakup of an air bubble injected into a fully developed turbulent flow. Part 2. Size PDF of the resulting daughter bubbles, " J. Fluid Mech. 401, 1999, pp.183– 207.
[40] W. Zhoua, Y. Yanb, Y. Xiea, and B. Liua , "Three-dimensional lattice Boltzmann simulation for mixed convection of nanofluids in the presence of magnetic field, " International Communications in Heat and Mass Transfer. 80, 2017, pp. 1-9.
[41] M. K. Trivedi, R. M. Tallapragada, A. Branton, D. Trivedi, G. Nayak, O. Latiyal, and S. Jana, "Evaluation of Atomic, Physical, and Thermal Properties of Bismuth Oxide Powder: An Impact of Biofield Energy Treatment, " American Journal of Nano Research and Applications. 3, 2015, pp.94-98.